MWIR–Visible Dual-Channel Airborne Imaging integration for High-Resolution Urban Mapping

Yanning Wang[1]
[1]Beijing University of Civil Engineering and Architecture, Beijing, China - 1108160025018@stu.bucea.edu.cn

Keywords: Airborne sensor integration, MWIR imaging, Aerial camera, GNSS/IMU synchronization, Multi-modal fusion

Abstract

High-resolution airborne remote sensing increasingly requires the coordinated acquisition of geometric and thermal information for applications such as urban infrastructure inspection, environmental monitoring, and emergency response. However, conventional airborne systems typically operate optical and thermal sensors as loosely coupled subsystems, leading to temporal misalignment, unstable geometric relationships, and limited consistency in fused products.

This paper presents EagleFrame IR-VM28K, a tightly coupled airborne MWIR–visible–GNSS/IMU integrated system designed for high-resolution thermal–optical observation. The system integrates a cooled mid-wave infrared (MWIR) imaging subsystem, a high-resolution visible dual-camera subsystem, and an AP+30 GNSS/IMU navigation unit under a unified mechanical structure, electrical control, and timing framework. A resolution-aware imaging strategy based on sweeping acquisition is adopted to enhance the effective thermal representation capability of the MWIR subsystem.

A unified processing workflow is established, including hardware synchronization, trajectory post-processing, installation-parameter calibration using POSPAC CalQC, MWIR radiometric correction, geometric reconstruction, cross-modal co-registration, and fusion. Furthermore, a multi-temporal thermal analysis framework is introduced to characterize thermal inertia and temporal thermal evolution of urban surfaces.

Flight experiments over Wujin District demonstrate that the proposed system achieves strong spatial consistency between visible and MWIR imagery and effectively represents thermal characteristics of roofs, pavements, and water bodies. Comparative analysis shows that tightly coupled integration and calibration significantly improve cross-modal alignment and fusion quality. The results confirm that the proposed system provides a robust solution for high-resolution airborne thermal–optical remote sensing and offers a foundation for thermal anomaly detection and urban thermal process analysis.

1. Introduction

With the continuous expansion of high-resolution remote sensing in urban governance, infrastructure inspection, ecological monitoring, and emergency management, the requirements for airborne payloads have evolved from purely geometric acquisition toward coordinated observation of geometric, radiometric, and thermal information. Visible aerial imagery provides high spatial resolution, clear object boundaries, and rich texture information, making it indispensable for precision mapping and object recognition. Mid-wave infrared remote sensing, in contrast, directly represents thermal radiation patterns of ground objects and provides a unique information source for heat leakage detection, temperature contrast analysis, thermal anomaly identification, and surface energy-process studies. The realization of synchronized acquisition, unified georeferencing, and accurate fusion of high-resolution visible and thermal infrared data on an airborne platform has therefore become a key development direction for multimodal remote sensing systems (Thiele et al., 2021).

In existing airborne multi-sensor systems, optical cameras and thermal infrared sensors are usually mounted and operated as relatively independent subsystems (Thiele et al., 2021). Although such configurations offer some engineering flexibility, they also introduce several challenges. First, differences in trigger mechanisms and exposure timing often cause temporal offsets between sensors. Second, the distributed installation of multiple devices makes it difficult to maintain stable lever-arm offsets and installation angles, and geometric inconsistency between modalities may arise under vibration, temperature variation, and structural deformation during flight. Third, differences in spatial resolution, field of view, spatial response, and imaging mechanism significantly increase the difficulty of subsequent multimodal registration and fusion. Under high-resolution airborne conditions, these problems directly affect the geometric accuracy and interpretability of thermal–optical integrated products.

In addition, airborne thermal remote sensing has long been constrained by the trade-off among detector performance, spatial resolution, and swath width. Although uncooled infrared systems are convenient for lightweight deployment, they are often insufficient in thermal sensitivity, signal-to-noise ratio, and thermal edge clarity for fine-scale thermal process recognition. By contrast, cooled MWIR detectors provide clear advantages in subtle temperature-difference detection, radiometric stability, and thermal anomaly identification, making them more suitable for high-precision airborne thermal remote sensing. However, practical use of cooled MWIR systems also places higher demands on platform integration, timing synchronization, attitude stability, and geometric calibration.

To address these issues, this paper develops EagleFrame IR-VM28K, an integrated airborne sensor system for high-resolution remote sensing. The system tightly integrates a cooled MWIR imaging subsystem, a high-resolution visible dual-camera subsystem, and an AP+30 GNSS/IMU device under a unified hardware triggering and airborne installation framework, thereby establishing a tightly coupled relationship among thermal, optical, positional, and attitudinal information. To ensure geometric accuracy, the study further introduces the scientific calibration workflow supported by POSPAC and CalQC, enabling joint estimation, refinement, and correction of lever-arm offsets and boresight angles. The paper focuses on system architecture, calibration methodology, data processing workflow, and flight experiment results, aiming to provide a practical reference for engineering applications of high-resolution thermal–optical airborne remote sensing systems.

The main contributions of this study are as follows:

(1) A tightly coupled MWIR–visible–GNSS/IMU airborne integration framework is proposed, ensuring temporal synchronization and geometric consistency among heterogeneous sensors;
(2) A resolution-aware thermal–optical fusion strategy is developed, considering differences in spatial response and effective thermal representation capability;
(3) A unified calibration workflow integrating trajectory post-processing and installation-parameter refinement (lever-arm and boresight) is established for multi-sensor systems;
(4) A multi-temporal thermal analysis approach is introduced to characterize thermal inertia and temporal thermal evolution of urban surfaces, enhancing the interpretability of fused products.

2. System Design and Methodology

2.1 Overall system architecture

EagleFrame IR-VM28K is an airborne integrated sensor system designed for high-resolution thermal–optical remote sensing. Its structure is shown in Figure 1, and the device parameters are listed in Table 1. It consists of three core subsystems: a cooled MWIR imaging subsystem, a high-resolution visible dual-camera subsystem, and a GNSS/IMU navigation subsystem. The entire system is rigidly integrated in a unified payload structure. All subsystems follow an integrated design principle in terms of mechanical installation, power control, trigger timing, and unified time reference, thereby reducing the instability of relative positions, temporal misalignment, and fragmentation of multi-source data processing commonly found in loosely coupled airborne payloads (Pöppl et al., 2025).

Unlike conventional “camera payload plus independently recorded navigation” configurations, the present system emphasizes both pre-designed geometric control and post-flight calibration refinement. By unifying installation references, trigger timing, and data time standards during system design, and by introducing high-precision trajectory processing and installation-parameter refinement in post-processing, the system forms a workflow from hardware integration to geometric calibration and fused-product generation.

Figure 1. IR-VM28K system

Module	Technical parameter	Specification
MWIR imaging	Original detector format	512 × 640
	Spectral range	3.7~4.8μm
	Equivalent strip sweeping image size	28,000 × 640
	Pixel size	15 μm
	Focal length	400 mm
	Total field of view	60°
	Minimum scan time	1.2 s
	NETD	80 mK
	IFOV	37.5 μrad
Visible imaging	Single-camera format	14,206 × 10,656
	Stitched image size	20,000 × 14,000
	Pixel size	3.76 μm
	Focal length	90 mm
	Exposure interval	0.5 s
	Shutter speed	1/2500 s
FMS & Navigation	Navigation	EagleFrame Navigator
	GNSS/IMU	AP+30

Table 1. Technical specifications of the IR-VM28K system

2.2 MWIR imaging subsystem

The MWIR subsystem is the thermal sensing core of EagleFrame IR-VM28K. It uses a cooled mid-wave infrared focal plane array with an original detector format of 512 × 640 pixels, a pixel size of 15 μm, a focal length of 400 mm, and a total field of view of 60°. The system has an NETD of 80 mK and an IFOV of 37.5 μrad. Data are recorded in 16-bit RAW format.

Because the original MWIR focal plane array is relatively limited in size, a conventional static frame-imaging mode would not be able to satisfy both wide-area coverage and high-resolution thermal imaging. To solve this problem, the system adopts a precision sweeping and stare-compensation imaging

https://doi.org/10.5194/isprs-archives-XLIX-B1-2026-113-2026

mechanism. In this mode, each strip consists of 62 consecutive imaging units, with a minimum scan time of approximately 1.2 s, resulting in an equivalent strip format of about 28,000 × 640 pixels. The schematic diagram of data acquisition is shown in Figure 2. This design significantly increases the across-track thermal coverage and improves the effective spatial representation of thermal patterns after geometric reconstruction.

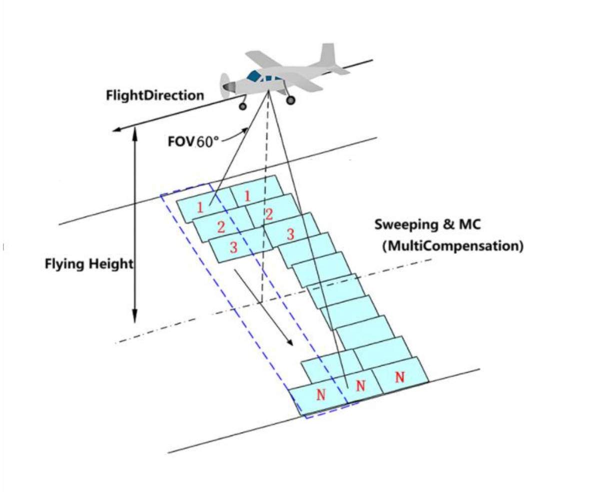

Figure 2. Sweeping operation and imaging geometry of the MWIR–optical integrated system

2.3 Visible dual-camera subsystem

The visible subsystem consists of RGB cameras. Each camera has an image format of 14,206 × 10,656 pixels, a pixel size of 3.76 μm, and a 90 mm lens. After image stitching, the subsystem forms an effective format of approximately 20,000 × 14,000 pixels, increasing both coverage and high-resolution geometric representation capability. The minimum exposure interval is 0.5 s, and the shutter speed can reach 1/2500 s, meeting the requirements of sharp imaging during high-speed airborne operation.

Within the integrated system, the visible subsystem not only performs the primary mapping-image acquisition task, but also acts as the main geometric reference for high-precision thermal–optical co-registration and target localization. High-resolution visible imagery provides clear object boundaries, material textures, and structural information, allowing MWIR thermal anomalies to be associated with real physical objects and thereby improving the interpretability of fused thermal–optical products.

2.4 Flight management and navigation subsystem

Flight management is performed by EagleFrame Navigator, which is used for mission planning, flight-line execution control, and coordinated sensor operation. The application of the Flight Management System (FMS) and Inertial Measurement Unit/Global Navigation Satellite System (IMU/GNSS) in flight operations is shown in Figure 3. The GNSS/IMU subsystem uses AP+30, which provides high-precision position, velocity, and attitude information and forms the basis for unified georeferencing and accurate geometric reconstruction.

Figure 3. FMS & IMU/GNSS in test flight operation

The significance of using AP+30 lies not only in the high-precision characteristics of the hardware itself, but also in its compatibility with mature post-processing tools such as POSPAC MMS and CalQC, enabling a scientific, standardized, and repeatable workflow for installation-parameter calibration. In airborne multi-sensor systems, spatial offsets and installation-angle differences between sensors are unavoidable. The translational offsets between sensor reference centers and the navigation reference point are defined as lever-arm offsets, while the angular differences between sensor coordinate frames and the navigation frame are defined as boresight angles. These parameters directly affect the correctness of exterior orientation recovery and are essential for high-precision unified representation of multimodal data.

3. Data Processing Workflow

3.1 Overall Workflow of Thermal-Optical Integrated Processing

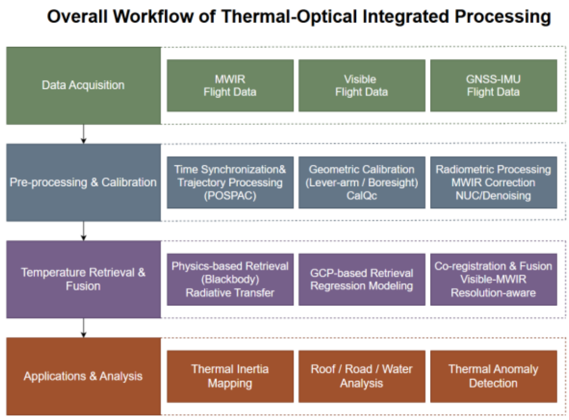

Figure 4. Overall workflow

3.2 Trajectory post-processing

The overall data processing procedure is depicted in Figure 4.After flight, GNSS/IMU data recorded by AP+30 are post-processed using POSPAC to produce high-precision position and attitude solutions. The flight path is shown in Figure 5.These post-processed navigation results form the basis for unified georeferencing of visible and MWIR imagery and also serve as the input for the CalQC installation-parameter calibration(Sampath, 2024). With this tool, the system forms a solution from trajectory estimation, installation-parameter refinement, and geometric reconstruction.

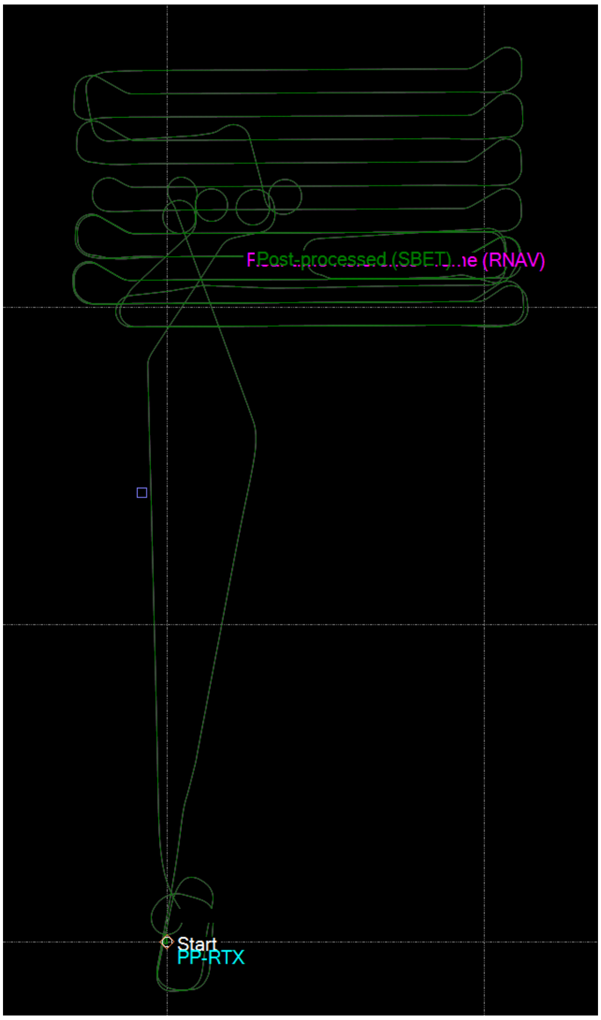

Figure 5. Post processed trajectory

3.3 Calibration principle

The geometric accuracy of an airborne integrated sensor system depends not only on the performance of individual sensors, but also on how well the geometric relationships among the subsystems are determined. In EagleFrame IR-VM28K, the MWIR subsystem, the visible dual-camera subsystem, and the AP+30 navigation unit form a typical rigidly coupled multi-sensor system. If the lever-arm offsets and boresight angles are not accurately estimated, even a highly precise navigation solution can still lead to significant positional and attitude errors after ground projection, thereby degrading cross-modal registration accuracy and the reliability of fused results.

The main objectives of system calibration are therefore:

(1) to determine the lever-arm offsets of the MWIR and visible subsystems relative to the AP+30 navigation reference frame;

(2) to calibrate and correct the boresight angles of each imaging subsystem relative to the navigation frame; and

(3) to establish a unified geometric reference suitable for multimodal airborne sensor systems.

3.4 Lever-arm offset calibration

Lever-arm offsets describe the spatial translation between each sensor reference center and the GNSS/IMU reference point, usually along the three axes of the aircraft body frame. For a system that combines a stitched visible dual-camera structure and an independent MWIR optical path, lever-arm offsets determine not only the exterior orientation recovery of each subsystem, but also the spatial consistency between different modalities.

Figure 6. Test flight over Wujin District

After system installation, initial lever-arm parameters are first established by mechanical measurement. Then, using the high-precision trajectory and attitude data recorded by AP+30, a joint geometric analysis of the flight data is carried out within the POSPAC framework, and the lever-arm parameters are calibrated and refined using CalQC. Essentially, this procedure constrains the mechanically measured initial values together with the optimal geometric relationships observed during real flight, thereby yielding corrected lever-arm values that better reflect the true operational state of the payload.

Lever-arm model: $\mathbf{X}_C = \mathbf{X}_{IMU} + \mathbf{R}_{IMU} \cdot \mathbf{l}$

Where: $\mathbf{X}_C = [X_C, Y_C, Z_C]^T$ Camera perspective center coordinates in the mapping reference frame

$\mathbf{X}_{IMU} = [X_{IMU}, Y_{IMU}, Z_{IMU}]^T$IMU position obtained from the post-processed trajectory (SBET)

$\mathbf{R}_{IMU}$ Rotation matrix transforming vectors from the IMU body frame to the mapping reference frame

$\mathbf{l} = [l_x, l_y, l_z]^T$Lever-arm offset vector from the IMU origin to the camera perspective center, expressed in the IMU body frame

3.5 Boresight caculation

Boresight angles describe the angular relationship between the sensor coordinate frame and the navigation reference frame, typically including roll, pitch, and heading components. In high-resolution airborne remote sensing, even very small boresight errors may propagate into significant planimetric and vertical deviations due to flight altitude, and their influence is particularly critical for thermal–optical integrated products.

In this study, the POSPAC CalQC workflow is employed. Flight missions are designed with cross flight lines, opposite-direction flight lines, and sufficient overlap. Under these multi-view observation conditions, the residual distribution of corresponding features is analyzed, and boresight corrections for both the MWIR subsystem and the visible subsystem relative to the AP+30 reference frame are estimated. Compared with approaches relying only on mechanical installation-angle measurements, the CalQC-based post-flight calibration more effectively absorbs actual installation perturbations, airborne structural deformation, and systematic errors encountered during flight, thereby improving the reliability of the final geometric reconstruction. Boresight rotation model as below:

$$\mathbf{R}_C = \mathbf{R}_{IMU} \cdot \mathbf{R}_b$$
$$\mathbf{R}_b = R_z(\kappa)\, R_y(\phi)\, R_x(\omega)$$

Where: $\mathbf{R}_C$ Rotation matrix from the mapping reference frame to the camera coordinate system $\mathbf{R}_{IMU}$Rotation matrix from the mapping reference frame to the IMU body frame ， $\mathbf{R}_b$ Boresight rotation matrix describing the misalignment between the IMU and camera coordinate systems ， ω Boresight angle around the X-axis (roll) ， ϕ Boresight angle around the Y-axis (pitch) ， κ Boresight angle around the Z-axis (yaw) ， $R_x(\cdot), R_y(\cdot), R_z(\cdot)$ Elementary rotation matrices around the X, Y, and Z axes, respectively. Figure 7 depicts the extraction of tie points and GCPs at the calibration site.

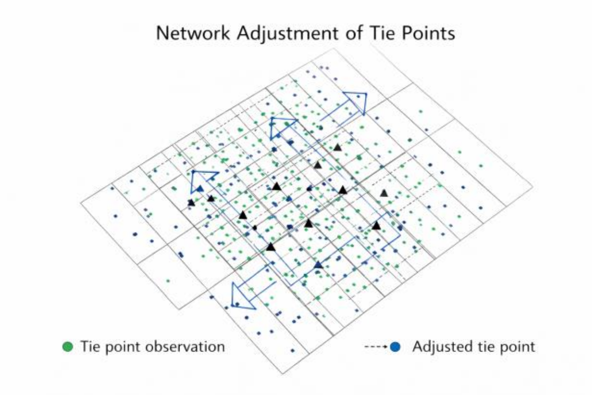

Figure 7. Calibration site Tie points and GCPs Extraction

3.6 Role of calibration results

The refined lever-arm offsets and boresight corrections produced by POSPAC CalQC are used as unified input parameters for subsequent geometric correction and multimodal fusion. For visible imagery, these parameters directly determine the accuracy of exterior orientation recovery. For MWIR imagery, they affect not only the geolocation accuracy of the thermal data itself, but also its spatial consistency with the visible products. Corrected exterior orientation as below:

$$EO_{corrected} = EO_{POS} + \Delta EO$$

Where: $EO_{corrected}$ Corrected exterior orientation parameters after calibration EO_{POS} Initial exterior orientation derived from POS processing (SBET) ΔEO Correction term estimated through bundle adjustment, including: Lever-arm corrections $\Delta \mathbf{l}$ Boresight angle corrections $\Delta\omega, \Delta\phi, \Delta\kappa$

To ensure temporal consistency among visible imagery, MWIR data, and navigation measurements, the system adopts a unified hardware triggering mechanism so that the imaging subsystems and AP+30 operate under a common timing reference. This design effectively reduces timing errors caused by trigger delay, exposure phase mismatch, and independent clock drift, thereby providing a reliable basis for subsequent geometric reconstruction and cross-modal registration.

3.7 MWIR radiometric correction and geometric reconstruction

Before fusion, MWIR data undergo radiometric consistency processing and geometric reconstruction. Radiometric correction is used to suppress detector non-uniformity, improve the stability of thermal information, and enhance thermal edge representation. Geometric reconstruction is carried out using the AP+30 post-processed navigation solution together with the refined installation parameters, allowing the MWIR data to be projected into a unified geographic framework. The rapid mosaicking of MWIR imagery is presented in Figure 8.

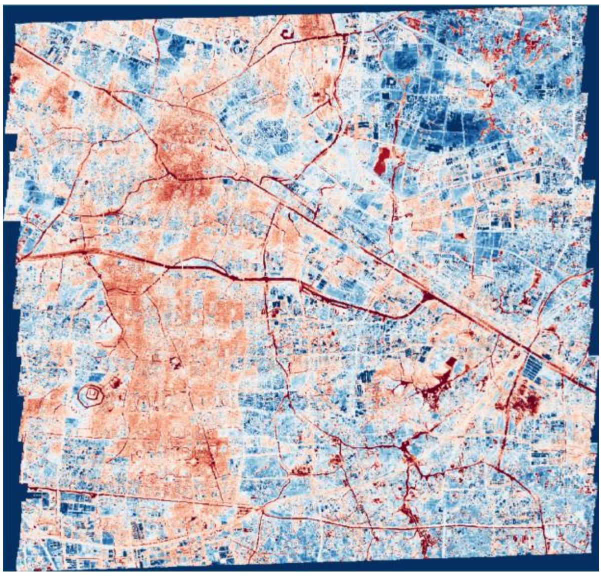

Figure 8. Rapid mosaicking of MWIR

3.8 Visible image reconstruction and cross-modal registration

Visible dual-camera data are processed to recover the exterior orientation of each image and then stitched into a high-resolution geometric reference base. The DOM of the AOI is presented in Figure 9.Subsequently, the visible imagery serves as the principal spatial reference for the MWIR data. Cross-modal registration and fusion are then carried out based on the georeferenced MWIR results. Since the two sensor types differ significantly in imaging mechanism, spatial response, and radiometric characteristics, the proposed approach uses a combined strategy based on a unified geometric framework and multimodal feature correspondence, rather than simple overlay of raw pixels.

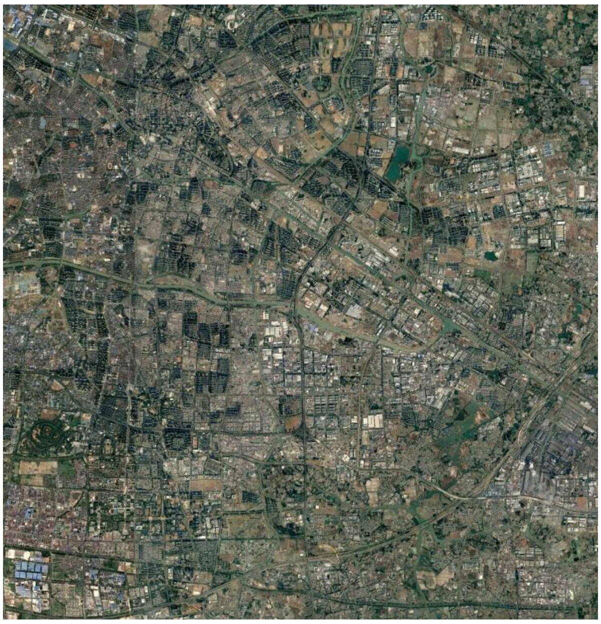

Figure 9. DOM of AOI

3.9 Generation of fused products

On the basis of unified georeferencing and corrected installation parameters, visible–MWIR fused products are generated. Figure 10 displays the visible RGB and thermal heatmap.The fusion strategy follows the principle that visible imagery provides the geometric framework, while MWIR imagery provides the thermal information basis. By combining unified grid representation with multimodal feature linkage, the system jointly characterizes structural and thermal information of ground objects, thereby providing a reliable data basis for later analyses of roof heat leakage, pavement temperature differences, and water-surface thermal gradients.

The fusion process follows a resolution-aware strategy in which visible imagery provides the geometric framework, while MWIR imagery contributes thermal information. Instead of treating the two modalities as equivalent pixel-level datasets, the method respects their different spatial responses and integrates them under a unified geometric reference.

A simplified fusion representation can be expressed as:

$$F(x, y) = G(x, y) + \lambda \cdot T(x, y)$$

where $G(x, y)$ represents geometric information derived from visible imagery, $T(x, y)$ represents thermal information from MWIR data, and λ is a weighting factor controlling the contribution of thermal features.

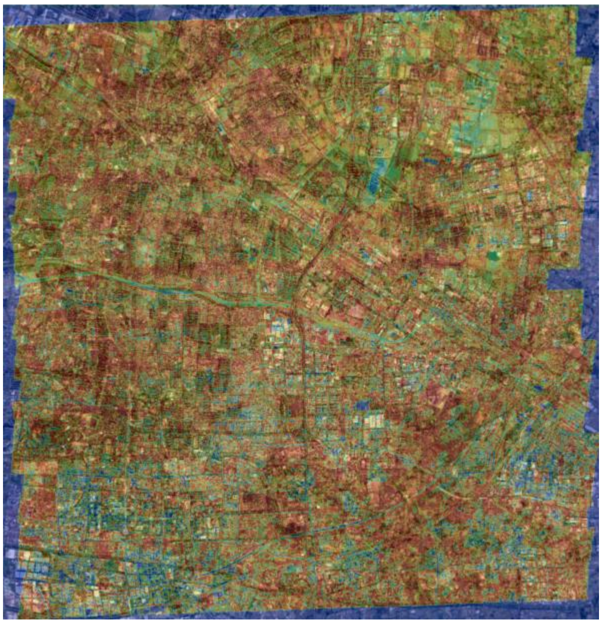

Figure 10. Visible RGB+ Thermal heatmap

4. Fusion Representation

It should be noted that the resolution metrics of the MWIR and visible subsystems correspond to their respective typical operating configurations. The MWIR subsystem demonstrates its thermal-imaging design capability, while the visible subsystem demonstrates its mapping-oriented geometric capability with the same. In engineering practice, the two subsystems do not need to operate with identical native imaging parameters; instead, they are integrated under a unified geometric framework according to task requirements.

4.1 Fusion representation principle

A unified analysis grid does not imply that the MWIR and visible channels are physically equivalent at the raw sensing level. The visible channel has stronger geometric boundary representation, whereas the MWIR channel is more focused on stable thermal-radiation sensing. Therefore, the fusion strategy follows the principle that visible imagery provides the structural framework and MWIR imagery provides the thermal basis, enabling coordinated thermal–optical representation under a unified geometric reference rather than treating the two datasets as structurally identical pixel sets.

4.2 Discussion of spatial-response differences

Although the fused products are represented on a unified analysis grid, the MWIR and visible channels still differ in spatial response, edge sharpness, and effective point spread characteristics. Therefore, the interpretation of thermal anomaly boundaries and their spatial extent must still consider the actual response capability of the MWIR subsystem. This treatment is more consistent with the physical properties of multimodal airborne remote-sensing products and helps improve the scientific rigor of result interpretation.

4.3 Multi-temporal Thermal Analysis

To further exploit the capability of MWIR sensing, a multi-temporal thermal analysis framework is introduced. Thermal observations acquired at different time periods (e.g., daytime, evening, and nighttime) are used to characterize the temporal evolution of surface temperature.

Let T(t, x, y) denote the temperature at time t and location (x, y). A thermal inertia indicator can be defined as:

$$\mathrm{TI}(x, y) = \mathrm{T\_day}(x, y) - \mathrm{T\_night}(x, y)$$

where T_day and T_night represent temperature observations during daytime and nighttime, respectively.

This indicator reflects the heat storage and release characteristics of different land-cover types. In general, built-up areas exhibit higher thermal inertia due to their material properties, while vegetation and water bodies show faster cooling behavior.

The multi-temporal analysis enhances the discrimination of urban surface types (Li et al., 2022) and provides a physically meaningful interpretation of thermal–optical fused products.

5. Experimental Verification and Result Analysis

5.1 Test area and objectives

Flight experiments were conducted in March over Wujin District, Changzhou city, Jiangsu Province, China. The real flight situation is shown in Figure 6. Figure 11 shows the workflow for the test area.The objectives were to verify:

(1) the spatial consistency between thermal and visible imagery;
(2) the capability of representing thermal characteristics of typical targets such as roofs, pavements, and water bodies;
(3) the practical effect of the AP+30 plus POSPAC CalQC calibration workflow on system geometric accuracy;
(4) the engineering feasibility of the integrated sensor system under real flight conditions.

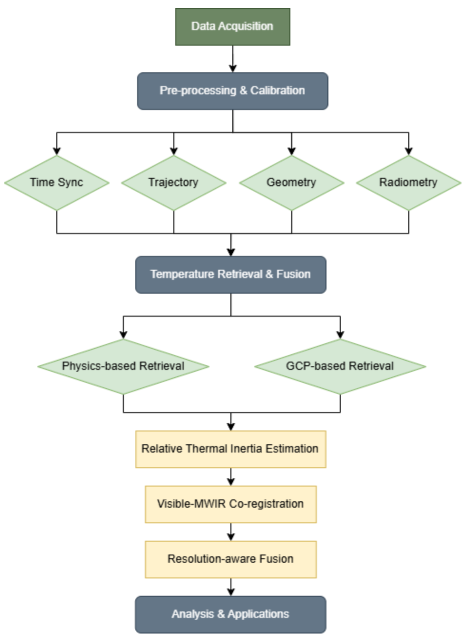

Figure 11. Test Area Workflow Diagram

5.2 Spatial consistency between visible and MWIR data

The results show that, after POSPAC post-processing and CalQC installation-parameter refinement, the visible and MWIR imagery achieve good spatial consistency over the full flight strip. Typical boundary features such as road edges, building outlines, shorelines, and vegetation patches maintain strong correspondence in both modalities, demonstrating that the rigid integrated installation and post-flight geometric calibration effectively reduce cross-modal misalignment.

5.3 Representation of roof heat leakage

Over building roofs, MWIR imagery clearly reveals temperature anomalies near roof edges, joints, and local structural transition zones. Combined with the high-resolution geometric detail of the visible images, these anomalies can be accurately linked to real building structures, thereby supporting roof insulation assessment and heat leakage inspection (Jiang et al., 2024).

5.4 Representation of pavement temperature variations

In road and paved-surface areas, the system identifies clear pavement temperature differences. Roads with different materials, heating histories, and local micro-environmental conditions exhibit distinct thermal-radiation responses in MWIR imagery, while the visible images provide precise spatial boundaries and contextual background for these thermal differences. This facilitates subsequent analysis of urban road thermal environments and pavement-condition assessment (Jiang et al., 2024).

5.5 Representation of water-surface cooling gradients

In water-body areas, the MWIR imagery continuously represents temperature gradients on the water surface and shows strong sensitivity to local cooling belts and heat-exchange boundaries. Combined with the shoreline, surrounding land cover, and environmental context derived from visible imagery, the system enhances the spatial interpretation of water thermal processes (Jiang et al., 2024).

5.6 Result analysis

The experimental results demonstrate that EagleFrame IR-VM28K not only supports coordinated acquisition of visible and MWIR data, but also establishes a stable and reliable system-level geometric relationship through the technical workflow based on AP+30 and POSPAC CalQC. This confirms that introducing mature navigation post-processing and calibration methods into a thermal–optical airborne integrated sensor system has significant value for improving multimodal spatial consistency and fusion quality.

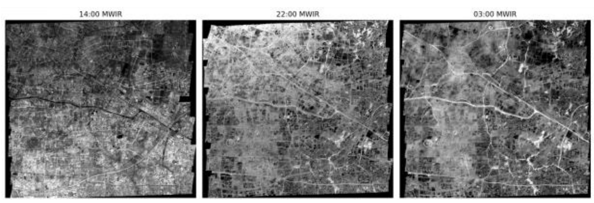

6. Conclusions and Future Work

The main contributions of this study are summarized as follows:

(1) Development of a compact and integrated airborne imaging platform using a cooled MWIR camera, substantially improving the effective spatial representation capability of airborne thermal imaging compared with conventional non-integrated configurations;

(2) Establishment of a unified workflow for synchronization, geometric calibration, and radiometric correction, ensuring consistent multi-sensor data fusion;

(3) Real-world flight validation demonstrating strong performance in geometric and thermal detail resolution, and real-scene application capability.

This system provides a valuable reference for the design of next-generation airborne remote sensing equipment that requires compact integration, high fidelity, and improved intelligence. The significant enhancement in thermal sensing capability, combined with precise optical-infrared alignment, demonstrates the potential of coordinated multi-sensor platforms in practical observation tasks. Future work may focus on integrating real-time onboard processing, incorporating machine learning techniques for automated thermal anomaly detection, and extending the system to support three-dimensional thermal mapping and long-term environmental monitoring. Such efforts will help advance the application of airborne sensing in natural resource management, urban digitalization, and emergency response, supporting more efficient and informed decision-making in complex environments.

References

Jiang, Z., et al., 2024. Research on cross-spatiotemporal remote sensing detection of marine oil spills and emulsions based on coupling optical and thermal response characteristics. IEEE Trans. Geosci. Remote Sens., 62, 1–12.

Li, D., et al., 2022. AGFP-Net: Attentive geometric feature pyramid network for land cover classification using airborne multispectral LiDAR data. Int. J. Appl. Earth Obs. Geoinf., 121, 102723.

Pöppl, F., Spitzer, A., Ullrich, A., Pfeifer, N., 2025. Airborne Laser Scanning for Corridor Mapping: Georeferencing with Tightly-coupled Multi-view LiDAR. Int. Arch. Photogramm. Remote Sens. Spatial Inf. Sci., XLVIII-1/W4, 109–114.

Sampath, A., 2024. Airborne lidar accuracy analysis for dual photogrammetric and lidar sensor pilot project in Colorado. U.S. Geol. Surv. Open-File Rep., 2024–1036.

Thiele, S.T., et al., 2021. Multi-scale, multi-sensor data integration for automated 3-D geological mapping. Ore Geol. Rev., 136, 104252.

Uciechowska-Grakowicz, A., et al., 2023. Usage of airborne LiDAR data and high-resolution remote sensing images in implementing the smart city concept. Remote Sens., 15(24), 5776.